JVST A
Journal of Vacuum Science & Technology A

ARTICLE

avs.scitation.org/journal/jva

Deposit and etchback approach for ultrathin Al_2O_3 films with low pinhole density using atomic layer deposition and atomic layer etching

Cite as: J. Vac. Sci. Technol. A 39, 062602 (2021); doi: 10.1116/6.0001340
Submitted: 6 August 2021 · Accepted: 11 October 2021 ·
Published Online: 5 November 2021

Jonas C. Gertsch,[1] Emanuele Sortino,[2] Victor M. Bright,[2] and Steven M. George[1]

AFFILIATIONS

[1]Department of Chemistry, University of Colorado, Boulder, Colorado 80309
[2]Department of Mechanical Engineering, University of Colorado, Boulder, Colorado 80309

Note: This paper is part of the 2022 Special Topic Collection on Atomic Layer Etching (ALE)

ABSTRACT

Ultrathin Al_2O_3 atomic layer deposition (ALD) films with low pinhole density were fabricated using a deposit and etchback approach. This strategy was able to avoid the pinholes that originated during nonuniform nucleation of Al_2O_3 ALD films. In this method, an Al_2O_3 ALD film was deposited to a thickness greater than the desired thickness to reduce the number of pinholes and form a more continuous Al_2O_3 ALD film. Subsequently, the Al_2O_3 ALD film was etched back to a smaller thickness using thermal Al_2O_3 atomic layer etching (ALE). The number of pinholes in the resulting Al_2O_3 ALD film was measured by the percentage yield of metal-insulator-metal (MIM) capacitors based on an $Ag/Al_2O_3/Al$ structure that did not have an electrical short. The device yield was improved using the deposition and etchback approach. For example, using device areas of 0.01 mm^2, Al_2O_3 ALD films that were grown to 5 nm in the MIM capacitor gave a yield of 30%–40%. In contrast, Al_2O_3 ALD films that were grown to 24 nm and then etched back to 5 nm to form the MIM capacitor provided a yield of 65%–75%. This increase in yield of approximately 100% indicates that the deposit and etchback approach can improve the yield of MIM devices based on ultrathin Al_2O_3 ALD films. Although this method has been previously suggested to improve the quality of ultrathin films, this report is believed to be the first demonstrated application of using the deposit and etchback approach for device fabrication. Additional experiments revealed that a portion of the yield improvement can be attributed to the fluorination of the Al_2O_3 ALD films that produced a volume expansion when forming AlF_3. This expansion may produce a compressive stress that helps to close the pinholes. The dielectric constant was also measured for Al_2O_3 ALD films versus Al_2O_3 film thickness. The dielectric constant was the same for as-deposited Al_2O_3 ALD films and Al_2O_3 ALD films that were first grown to 24 nm and then etched back to smaller thicknesses. This agreement indicates that the dielectric constant can be understood in terms of a series capacitor model and that Al_2O_3 ALE does not affect the electrical properties of the Al_2O_3 films.

I. INTRODUCTION

Atomic layer deposition (ALD) is a preferred method for depositing dielectric films because of the resulting superior thickness control and conformality on many surfaces.[1] Deposition of Al_2O_3 is one of the most studied ALD systems.[1,2] Al_2O_3 ALD films are important for device fabrication because they have a reasonably high dielectric constant and good insulating behavior.[3] Al_2O_3 ALD can be deposited on Si with a very small interfacial layer.[4] Al_2O_3 also has a large band offset with respect to Si.[5] This band offset is important for low leakage currents through devices.[6] The Al_2O_3 ALD film also remains amorphous until high temperatures of $T > 800$ °C.[7,8]

Al_2O_3 ALD films are widely used for various purposes. Some examples include optical coatings,[9] gas diffusion barriers,[10,11] protective coatings,[12–14] and nucleation promoters.[15] Al_2O_3 ALD films can be used to tune resonance frequencies in MEMS oscillators.[16] Ultrathin Al_2O_3 ALD films are also important in metal-insulator-metal (MIM) structures,[17] in metal-oxide-semiconductor (MOS) capacitors,[18] or as tunneling barriers in Josephson junctions.[19] The applications for ultrathin Al_2O_3 ALD films are affected by nucleation difficulties and pinholes resulting from noncontinuous films. Metal oxide ALD can have poor nucleation on noble surfaces, such as Au and Pt, and can require many ALD cycles to overcome the

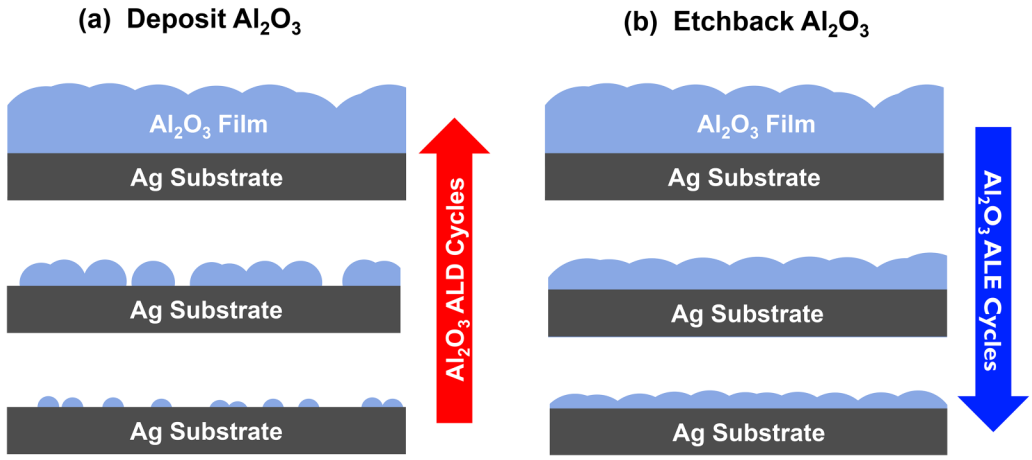

FIG. 1. Deposition and etchback schematic showing strategy for the fabrication of ultrathin films with low pinhole density.

incubation period.[3,20,21] These nucleation difficulties can lead to degraded electrical properties and poor insulating behavior for ultrathin Al_2O_3 ALD films.

Ultrathin, pinhole-free dielectrics are critical to future microelectronics as device layers continue to get thinner. New methods are required to minimize the pinholes in ultrathin Al_2O_3 ALD films. Recently, thermal atomic layer etching (ALE) has emerged as a method to remove thin films with atomic layer control.[22–24] Thermal ALE is based on sequential, self-limiting surface reactions and has been described as the "reverse of ALD."[24,25] Processes exist for the thermal ALE of a variety of materials, including Al_2O_3,[23,26] HfO_2,[27,28] SiO_2,[29] TiN,[30] Si,[31] Si_3N_4,[32] and W.[33] Thermal ALE has also been suggested as a method of improving ultrathin film quality by a deposition and etchback approach.[34] In this method, a film is grown to a thickness past its nucleation regime and then etched back to a desired thickness.[34] This process is illustrated in Fig. 1.

The deposition and etchback technique employing ALD and thermal ALE may allow for a thinner continuous film to be fabricated than by conventional ALD alone. The initial thicker films will eventually fill in the pinholes resulting from nucleation difficulties for ultrathin films. Subsequently, the thermal ALE can reduce the film thickness and often concurrently smooth the film.[27,35] This deposition and etchback process can produce thinner continuous films because the etchback may not reopen the pinholes. Similar to ALD, thermal ALE can also be utilized on high aspect ratio surfaces.[22] Consequently, the deposition and etchback approach could allow for pinhole reduction in ultrathin films on 3D surfaces. ALD is already used to fabricate high-aspect-ratio devices, such as in MIM-capacitor stacks in 3D silicon.[36,37]

In this paper, device yield improvements in MIM-type capacitors were observed using the deposition and etchback approach with Al_2O_3 ALD as the insulator layer. Improvement was also observed with hydrogen fluoride (HF) exposure. Al_2O_3 ALD films were deposited on silver (Ag) using trimethylaluminum (TMA) and de-ionized water (DI) at 130 °C.[38] Thermal ALE was performed with TMA and HF at 275 °C.[26] Aluminum (Al) was used as the top electrode. Device improvements were characterized by comparing as-deposited films to films of similar thicknesses that had been etched back from a thicker film thickness. Capacitance was also measured both for as-deposited films and for films after etching.

II. EXPERIMENT

A. Sample fabrication

Custom-fabricated MIM-type capacitors were used as the test devices. The fabrication process is shown in Fig. 2. A lift-off process using NR1500Y photoresist and standard photolithography was used to pattern an untreated 3 in. fused-silica glass wafer as shown in Fig. 2(a). The patterned photoresist was then used to deposit Ti/Ag pads of different areas as illustrated in Fig. 2(b). These electrical pads of different areas facilitated electrical testing of the capacitance and device yield as a function of the Al_2O_3 ALD film area.

The titanium (Ti) and silver (Ag) layers, with thicknesses of 10 and 90 nm, respectively, were deposited by thermal evaporation in an Edwards AUTO 306 vacuum coater at a pressure of 7.5×10^{-6} Torr. After the deposition, photoresist was removed using a cleaning procedure with sonication in acetone, isopropyl alcohol (IPA), and DI H_2O. The wafer was then diced into smaller samples that could fit into the ALD and ALE reactors.

The ALD process for Al_2O_3 films was conducted in a custom-built reactor at a reactor temperature of 130 °C.[39] TMA (97%, Aldrich) and DI H_2O were employed as coreactants. Dry nitrogen (N_2 99.999%, Airgas) was used as both a carrier and an inert purge gas with a constant flow of 160 SCCM. This N_2 carrier gas produced a reactor pressure of ~1 Torr. One ALD cycle consisted of a 3 s TMA exposure, a 55 s N_2 purge, a 3 s DI H_2O exposure, and a 55 s N_2 purge. After the Al_2O_3 ALD shown in Fig. 2(c), one set of the samples was annealed overnight in vacuum at 275 °C in a separate viscous flow reactor.[40] This thermal annealing was performed at the same temperature as the temperature used during Al_2O_3 ALE to avoid any artifacts due to thermal cycling.

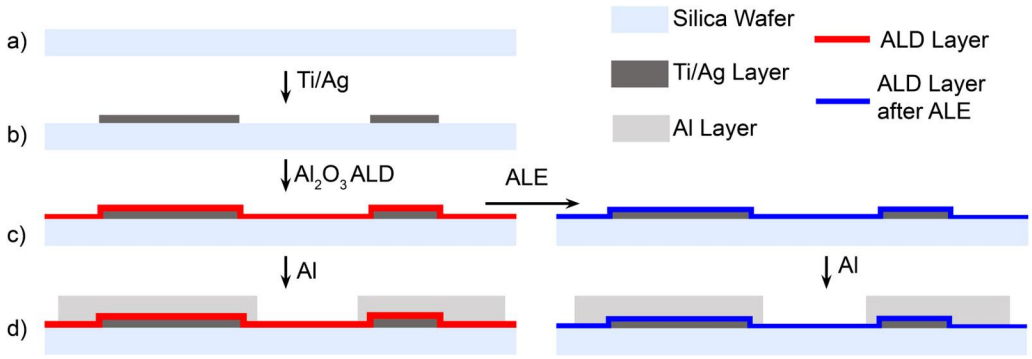

FIG. 2. MIM capacitor device fabrication process flow for the characterization of device yield.

After Al_2O_3 ALD, the other set of the samples was etched using Al_2O_3 ALE as shown in Fig. 2(c). The Al_2O_3 ALE process used TMA and HF (HF-pyridine, 70 wt. % HF, Sigma-Aldrich) as the reactants.[26] Etching occurred at 275 °C in the same reactor used to anneal the ALD films. One ALE cycle consisted of a 1.5 s TMA exposure, a 30 s N_2 purge, a 1 s HF exposure, and a 30 s N_2 purge. N_2 flow was kept constant at 150 SCCM during the ALE processing. The N_2 flow produced a reactor pressure of ~1 Torr. Under these conditions using HF pressures of 200–300 mTorr, the Al_2O_3 etch rate was ~0.5 Å/cycle in the steady-state regime in approximate agreement with earlier studies.[26,41]

Al_2O_3 ALD film thicknesses on Ag after deposition and after ALE were characterized by *ex situ* spectroscopic ellipsometry (SE, J. A. Woollam M-2000). The SE data were fit using CompleteEASE software (J. A. Woollam). The ellipsometer model used a fixed B-spline substrate layer for Ag. A Cauchy multisample analysis fit was used for the Al_2O_3 top layer. The model did not account for the thin AlF_3 surface layer that forms during etching. However, the thickness variation due to the thin AlF_3 layer was determined to be negligible.

After the Al_2O_3 ALD and anneal, or after the Al_2O_3 ALE, 250 nm of aluminum (Al) was then deposited as the top electrode of the MIM capacitor as shown in Fig. 2(d). This Al deposition was also performed by evaporation. The Al was patterned with a lift-off process similar to the Ti/Ag layer. Seven device areas were employed that ranged in size between 4×10^{-3} and 0.16 mm^2.

B. Sample characterization

Atomic force microscopy (AFM, Park Systems NX10) was used to measure the surface roughness of the samples. An OMCL-AC160TS (Park Systems) noncontact cantilever was employed for scanning. Measurements were recorded for the initial Ag-on-glass surface, the surface after depositing 24 nm of Al_2O_3 ALD, the Al_2O_3 surface after the 275 °C anneal and lift-off process, and the surface after etching 12 nm of Al_2O_3 by Al_2O_3 ALE. Al_2O_3 ALD films on Si wafers were also employed to compare with similar Al_2O_3 ALD films on Ag both before and after etching. Scan areas were $1 \times 1\,\mu m^2$ (512 pixels × 512 pixels). A scan rate of 0.25 Hz was used in noncontact mode. In addition, x-ray photoelectron spectroscopy (XPS, PHI 5600) was employed to measure atomic percentages after etching or after an extended HF exposure.

An LCR meter (BK Precision 895) was employed to measure the capacitance of the devices. Electrical contact was achieved using tungsten probes on manipulators. The probes made electrical connection on contact pads external to the device area to prevent any damage to the MIM device during measurement. The area of the MIM device was defined by the overlap of the Ag and Al electrodes. Capacitance measurements were recorded at 1 kHz and 1 V for 20 devices of each area size. Simultaneously, the resistance was measured as a proxy for shorted devices. The devices were considered shorted when the electrical resistance measured on the order of ~1 Ω. For working devices, the values obtained were above 1 MW or outside of the readable scale of the LCR meter.

The yield percentage was calculated as

$$\text{Yield}(\%) = \left(1 - \frac{\text{Number of shorted devices}}{\text{Number of tested devices}}\right) \times 100. \quad (1)$$

For film thicknesses under 5 nm, due to the different tunneling mechanisms, the yield was obtained with a source meter (Keithley 2400) applying a voltage of 1 V. The top Al layer was used as the positive electrode and the maximum current was limited at 105 μA.

The dielectric constant, ϵ_r, was then obtained using

$$\epsilon_r = \frac{Ch}{A\varepsilon_o}. \quad (2)$$

In this equation, C is the capacitance, h is the Al_2O_3 ALD film thickness, A is the measured device area, and ε_0 is the permittivity of free space.

III. RESULTS AND DISCUSSION

A. Al_2O_3 ALD and ALE

Ex situ SE was used to characterize the Al_2O_3 ALD growth on the initial Ag surface. The ellipsometry data for the Al_2O_3 ALD

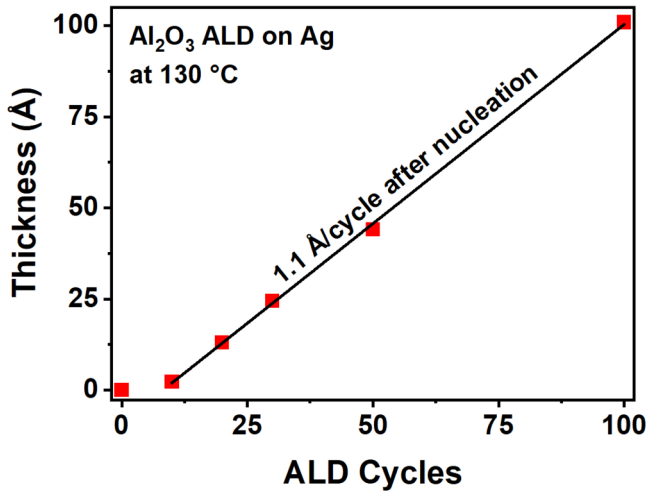

FIG. 3. Thicknesses measured by spectroscopic ellipsometry for Al_2O_3 ALD-on-Ag at 130 °C vs ALD cycles yielding a growth rate of 1.1 Å/cycle. Fit excludes the initial nucleation period.

film thickness versus number of ALD cycles is displayed in Fig. 3. Al_2O_3 ALD on Ag showed a slight nucleation delay of ~10 cycles. After the nucleation period, the average Al_2O_3 growth rate on Ag was 1.1 Å/cycle. This growth rate is characteristic of Al_2O_3 ALD.[2,38] The nucleation delay may indicate island or nonconformal growth during the first few ALD cycles. This nucleation delay could lead to pinholes in the ultrathin film.

The initial Ag surface after the evaporation deposition and lift-off process on glass was imaged with AFM as displayed in Fig. 4(a). The RMS roughness was 1.93 nm, and the rough surface morphology is visible in the AFM line scan immediately below the AFM image. Additional AFM images were used to characterize the Al_2O_3 surface as-deposited on Ag and after additional processing steps. All Al_2O_3 ALD films measured by AFM were deposited on Ag. Figure 4(b) shows the AFM image after the deposition of 24 nm of Al_2O_3 ALD at 130 °C but before annealing to 275 °C. The RMS roughness was reduced to 0.92 nm resulting from smoothing by the Al_2O_3 ALD film.[42,43] The line scan below the AFM image is noticeably smoother than the line scan in Fig. 4(a).

Figure 4(c) displays the AFM image after Al_2O_3 film annealing at 275 °C and after the photolithography lift-off and cleaning process following the Al electrode deposition. The Al_2O_3 surface was protected by photoresist during the Al electrode deposition. The photoresist was subsequently removed through a lift-off process. The Al_2O_3 film was very smooth after the 275 °C anneal with an RMS roughness of only 0.61 nm. This smoothing process could have been caused by a change in the underlying silver oxide interface layer, because the annealing temperature approached or exceeded the melting or decomposition temperature of silver oxide.[44,45] The line scan under the AFM image in Fig. 4(c) is consistent with a smoother surface.

Figure 4(d) shows the AFM image after the removal of 12 nm of the Al_2O_3 ALD film by Al_2O_3 ALE at 275 °C. This surface had an RMS roughness of 1.59 nm. The line scan under the AFM

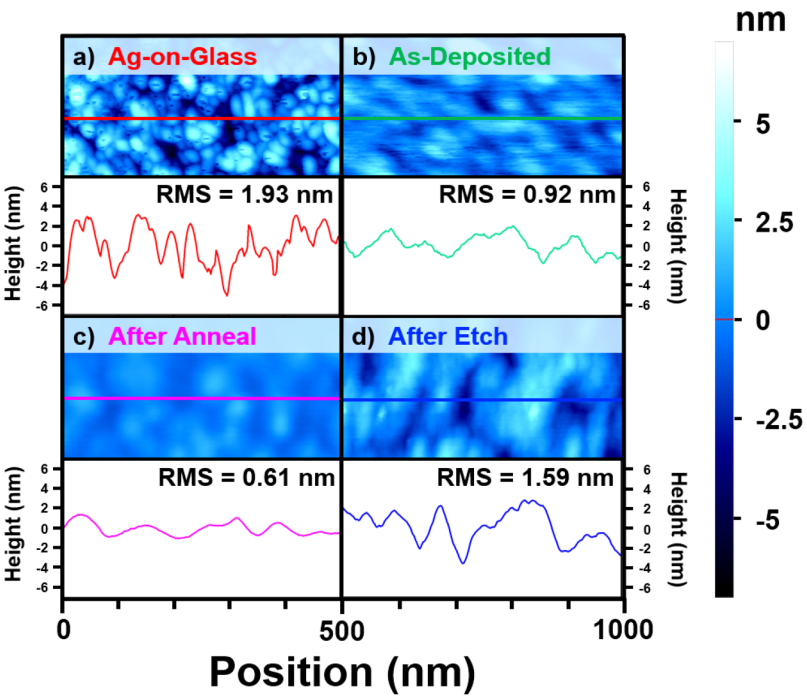

FIG. 4. AFM images and line scans of the (a) initial Ag surface, (b) Al_2O_3 surface after depositing 24 nm of Al_2O_3 ALD before annealing, (c) Al_2O_3 surface after annealing and lift-off processing, and (d) Al_2O_3 surface after removing 12 nm of Al_2O_3 by Al_2O_3 ALE.

image shows that the surface was smoother than the initial Ag film. However, the surface was rougher than the initial surface prior to Al_2O_3 ALE shown in Fig. 4(c). The slightly rougher surface after Al_2O_3 ALE was unexpected based on earlier results that have revealed that Al_2O_3 ALE can smooth Al_2O_3 surfaces.[23,35]

To test the ability of Al_2O_3 ALE to smooth Al_2O_3 surfaces, a 26 nm Al_2O_3 ALD film on Si with native oxide was used as a control to compare with Al_2O_3 ALD films deposited on Ag. The initial RMS roughness of the Al_2O_3 ALD film on the Si surface after a 275 °C anneal was only 0.15 nm. The Al_2O_3 surface remained smooth even after Al_2O_3 ALE removed 14 nm of the Al_2O_3 film. The RMS roughness of this Al_2O_3 surface after etching was only 0.14 nm.

The slight roughening of the Al_2O_3 ALD film on Ag after Al_2O_3 ALE may be attributed to the initial nucleation of Al_2O_3 ALD on Ag. The initial nucleation may have led to island growth and subsequent inhomogeneities in the Al_2O_3 ALD film.[3,20,21] If there were density inhomogeneities, then these density fluctuations may lead to differences in the Al_2O_3 etch rate and surface roughening. Earlier measurements of Al_2O_3 ALE for amorphous and crystalline Al_2O_3 ALD films revealed that the denser crystalline Al_2O_3 ALD films had much smaller etch rates.[8] In addition, the initial nucleation may also have produced variable local stresses in the Al_2O_3 ALD film that affected the etch rate. Al_2O_3 ALE involves fluorination and requires a significant volume expansion for Al_2O_3 to form AlF_3.[8,46] This volume expansion may be sensitive to the stress in the Al_2O_3 ALD film.

The Al_2O_3 surface deposited on Ag was also evaluated with AFM after an extended HF exposure at 275 °C. The fluorination consisted of three 10 s HF doses with 10 s N_2 purges separating each dose. No noticeable change in surface roughness was observed following this fluorination process. XPS was also used to analyze the atomic percentages of F, C, Al, and O on the surface of the Al_2O_3 films after the extended fluorination. No significant change in composition was observed when compared with Al_2O_3 ALD films after Al_2O_3 ALE that ended with an HF exposure. The fluorine atomic percentage agreed well with previous investigations.[41] In addition, XPS analysis of the Al_2O_3 ALD films after Al_2O_3 ALE revealed no nitrogen in the films.

B. Capacitance and dielectric properties of as-deposited Al_2O_3 films and after ALE

Capacitance measurements on Al_2O_3 ALD films of different areas are shown in Fig. 5. The expected linear relationship between capacitance and device area was observed for both the unetched and the etched films of different Al_2O_3 film thicknesses. The solid squares in Fig. 5 correspond to the as-deposited and annealed Al_2O_3 ALD films. The solid triangles correspond to the Al_2O_3 ALD films after Al_2O_3 ALE. The Al_2O_3 ALD films after Al_2O_3 ALE were etched back from initial Al_2O_3 ALD films with a thickness of 24 nm. Figure 5 shows that the Al_2O_3 ALE process has a negligible effect on the capacitance.

The average dielectric constant for the various film thicknesses is shown in Fig. 6. The dielectric constant starts at about $\epsilon_r = 4$ at low film thicknesses and increases progressively versus Al_2O_3 ALD film thickness. These data are compared with similar previous measurements of Al_2O_3 ALD films deposited at 177 °C on silicon and molybdenum substrates.[3] There is good agreement between the various dielectric values as a function of film thickness.

The increase in dielectric constant with increasing film thickness, along with a decrease in dielectric constant during etching as

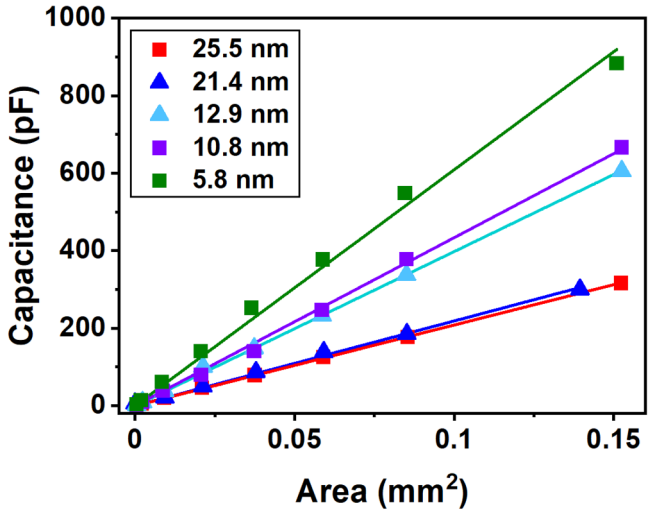

FIG. 5. Capacitance measurements for Al_2O_3 films of varying thicknesses. Closed squares correspond to annealed as-deposited Al_2O_3 ALD films. Closed triangles correspond to Al_2O_3 films that were etched back from an initial thickness of 24 nm using Al_2O_3 ALE.

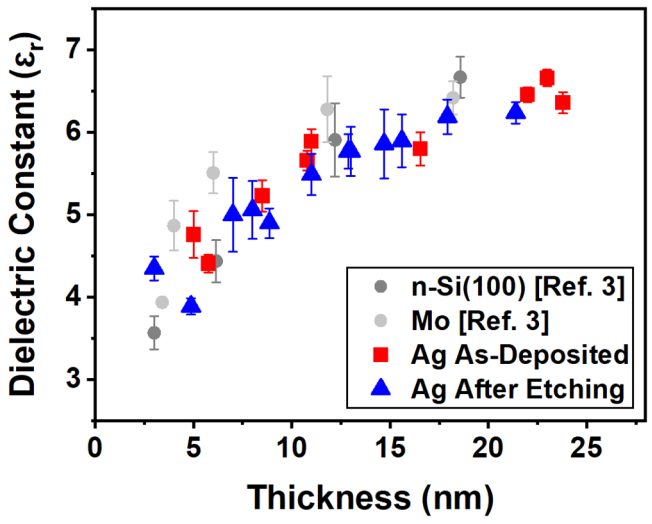

FIG. 6. Dielectric constant of Al_2O_3 ALD films on several different substrates vs film thickness. Solid squares correspond to as-deposited Al_2O_3 ALD films after annealing. Solid triangles correspond to Al_2O_3 ALD films that were etched back from an initial thickness of 24 nm using Al_2O_3 ALE. Solid circles are replotted from Ref. 3 for comparison.

the film thickness decreases, can be explained by the series capacitor model.[3] For two or more dielectrics in series, the equivalent capacitance is

$$\frac{1}{C_{eq}} = \frac{1}{C_1} + \frac{1}{C_2} + \ldots + \frac{1}{C_n}. \quad (3)$$

Dielectric constants were modeled using Eq. (2) based on the estimated equivalent capacitance from Eq. (3). The model results in Fig. 7 show an excellent fit to the experimental values both for the as-deposited Al_2O_3 ALD film thicknesses in Fig. 7(a) and for the Al_2O_3 ALD film thicknesses after Al_2O_3 ALE in Fig. 7(b). The model in Fig. 7(a) used Ag_2O and Al_2O_3 as two dielectrics in series. The model in Fig. 7(b) used Ag_2O, Al_2O_3, and AlF_3 as three dielectrics in series.

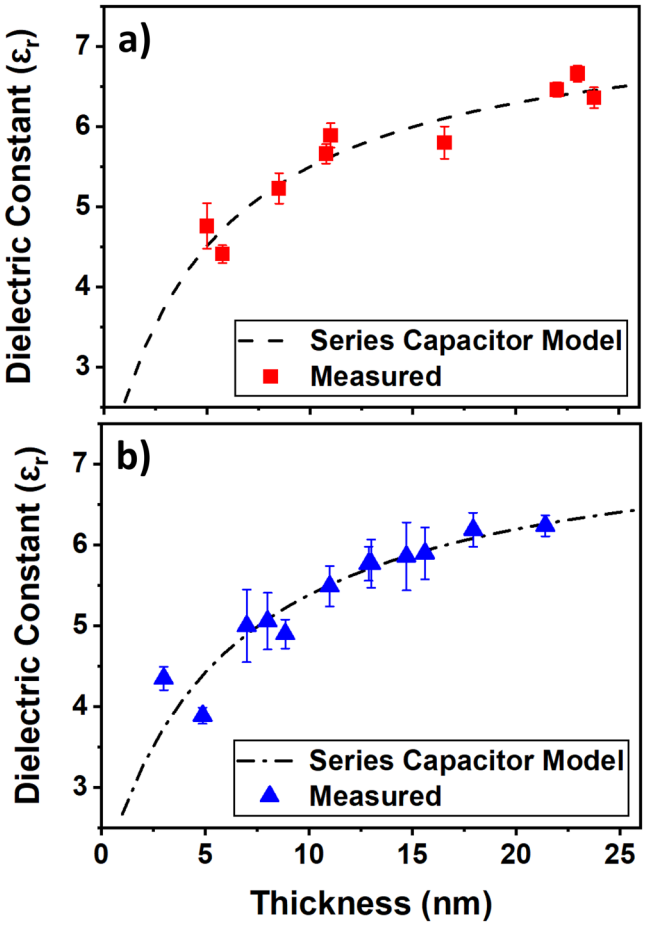

FIG. 7. Comparison of measured and model dielectric constants for Al_2O_3 ALD films on Ag. (a) Results for as-deposited Al_2O_3 ALD films after annealing and model for Ag_2O and Al_2O_3 as two dielectrics in series. (b) Results for Al_2O_3 ALD films that were etched back from an initial thickness of 24 nm using Al_2O_3 ALE and model for Ag_2O, Al_2O_3, and AlF_3 as three dielectrics in series.

The model results in Fig. 7 used an Ag native oxide thickness of 1.1 nm.[47] Dielectric constants for Ag_2O and Al_2O_3 were 1.6 and 7.5,[11,48,49] respectively. The model for the etched film also considered an additional AlF_3 layer with a dielectric constant of 3.4 and a thickness of 0.3 nm.[41,50] This layer formed during the Al_2O_3 ALE process on top of the Al_2O_3 layer. This low dielectric constant AlF_3 layer lowered the film permittivity by only ~4% after the Al_2O_3 ALE process. This AlF_3 layer could be avoided by ending the Al_2O_3 ALE process with an extended TMA exposure. Both models for the as-deposited and etched films used the same Al_2O_3 dielectric constant of $\epsilon_r = 7.5$.

C. Yield improvements for Al_2O_3 films after ALE

Figure 8 shows the percent yield of the measured devices per capacitor area for Al_2O_3 ALD film thicknesses of 8.8, 10.7, and 16.4 nm. The larger area devices were more likely to short. This behavior is consistent with pinholes or other defects that are causing device failures. For larger device areas, the probability of encountering a pinhole is higher. Consequently, the possibility of having a shorted device is also higher for larger device areas.[51]

The percent yield was then determined for as-deposited Al_2O_3 ALD films and Al_2O_3 ALD films grown to 24 nm and then etched back to obtain smaller thicknesses. A percent yield comparison between the as-deposited films and the films etched back from 24 nm is shown in Fig. 9. These results were for electrode pads with an area of 0.01 mm^2. These pad areas of 0.01 mm^2 showed the best contrast in yield between the as-deposited Al_2O_3 ALD films and films after Al_2O_3 ALE. The thicker as-deposited ALD films had higher percent yields. This behavior is attributed to a decrease in pinholes or other defects for thicker films that would expose the underlying electrode and lead to an electrical short.

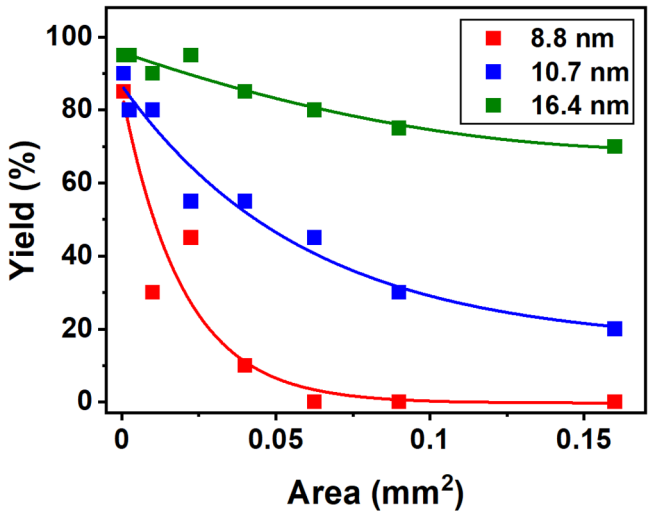

FIG. 8. Yield as a function of device area for Al_2O_3 ALD films with thicknesses of 8.8, 10.7, and 16.4 nm.

Figure 9 demonstrates that the device yield was improved using the deposition and etchback approach. For example, Al_2O_3 ALD films that were grown to 5 nm gave a yield of 30%–40%. In contrast, Al_2O_3 ALD films that were grown to 24 nm and then etched back to 5 nm provided a yield of 65%–75%. This improvement was an increase in yield by approximately 100% for the film thickness of 5 nm. This improvement was attributed to an irreversible closure of pinholes following the deposition and etchback process. After depositing a thick enough film, past the point where a pinhole would be covered, etching back to a thinner film did not reopen this pinhole. Alternatively, the closure of a pinhole could result from an effect of ALE processing such as fluorination. These results are believed to be the first demonstration of a deposit and etchback approach for device fabrication.

To explore these explanations further, as-deposited Al_2O_3 ALD films of varying thicknesses were etched only a small amount by the Al_2O_3 ALE process. The results shown in Fig. 10(a) indicate an increase in yield for all the etched devices. Some effects from the ALE process itself may improve the yield. The improvement in the yield may not be from only the deposition and etchback process illustrated in Fig. 1.

To test the effect of the ALE process, three Al_2O_3 ALD films of 12.2 nm thicknesses, annealed at 275 °C, were used for additional measurements. One Al_2O_3 ALD film sample was retained as a control. The second sample was exposed to three 10 s TMA doses, each separated by a 10 s N_2 purge, under the Al_2O_3 ALE conditions after the Al_2O_3 ALD. The third sample was exposed to three 10 s HF exposures, also separated by 10 s N_2 purges, under the Al_2O_3 ALE conditions after the Al_2O_3 ALD. The results displayed in Fig. 10(b) show a clear increase in yield for the Al_2O_3 ALD films exposed to HF. In contrast, the yield of the Al_2O_3 ALD films exposed to TMA did not vary significantly from the Al_2O_3 ALD control samples.

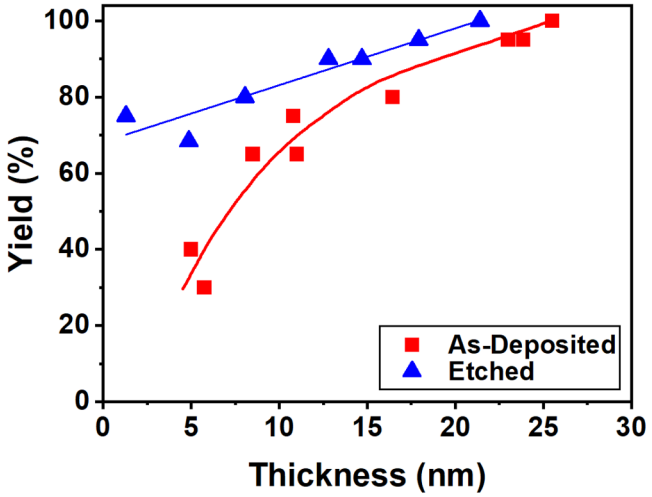

FIG. 9. Comparison in yield for Al_2O_3 ALD MIM-capacitor devices vs Al_2O_3 film thickness for as-deposited Al_2O_3 ALD films (solid squares) and Al_2O_3 films that were etched back from an initial thickness of 24 nm using Al_2O_3 ALE (solid triangles). Capacitor area was 0.01 mm^2.

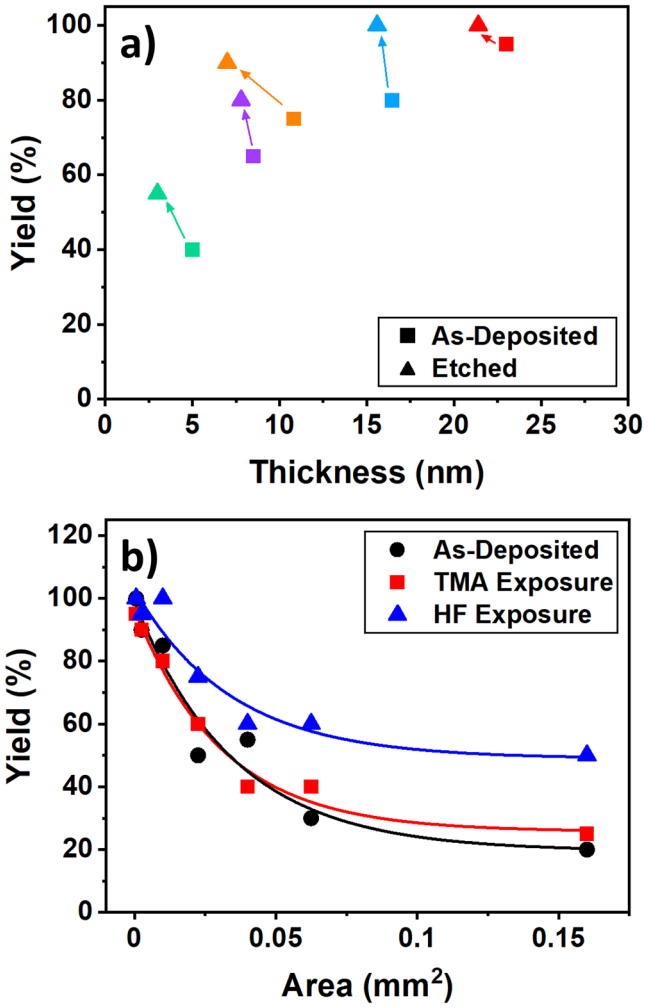

FIG. 10. (a) Yield after small number of Al_2O_3 ALE cycles for different Al_2O_3 ALD film thicknesses. (b) Yield as a function of device area for Al_2O_3 ALD films with thicknesses of 12.2 nm for as-deposited Al_2O_3 ALD films (solid circles), after additional TMA (solid squares) exposures, or after HF (solid triangles) exposures.

The increased yield for the devices exposed to HF may have resulted from the volume expansion that Al_2O_3 undergoes when converted to AlF_3.[46] The fluorinated Al_2O_3 layer on the Al_2O_3 ALD film has a thickness of 2–3 Å.[41] The estimated increase in volume for this AlF_3 layer is around 70% given an Al_2O_3 ALD density of 3.0 g/cm^3 and an AlF_3 density of 2.9 g/cm^3.[38,39] The volume expansion upon fluorination would produce a compressive stress in the AlF_3 film.[46] This compressive stress generated during conversion of Al_2O_3 to AlF_3 could help close cracks or pinholes and reduce the probability of a failed device.

IV. CONCLUSIONS

Ultrathin Al_2O_3 films with low pinhole density were fabricated using a deposit and etchback approach with Al_2O_3 ALD and thermal Al_2O_3 ALE. This strategy was able to reduce the number of pinholes in ultrathin films that originated during nonuniform nucleation. The existence of pinholes in the resulting Al_2O_3 ALD film was quantified by the percentage yield of metal-insulator-metal (MIM) capacitors based on an $Ag/Al_2O_3/Al$ structure that did not display an electrical short.

Using device areas of 0.01 mm^2, Al_2O_3 ALD films that were grown to 5 nm in the MIM capacitor gave a yield of 30%–40%. In contrast, Al_2O_3 ALD films that were grown to 24 nm and then etched back to 5 nm to form the MIM capacitor provided a yield of 65%–75%. This increase in yield of approximately 100% indicates that the deposit and etchback approach can improve the yield of MIM devices based on ultrathin Al_2O_3 ALD films. This improvement may be the first illustration of a deposit and etchback approach for device fabrication. Additional experiments revealed that a portion of the yield improvement can be attributed to the fluorination of the Al_2O_3 ALD films that produces a volume expansion when forming AlF_3. This expansion may produce a compressive stress that helps to close the pinholes.

The dielectric constant was also measured for Al_2O_3 ALD films versus Al_2O_3 film thickness. The dielectric constant was the same for as-deposited Al_2O_3 ALD films and Al_2O_3 ALD films that were first grown to 24 nm and then etched back to smaller thicknesses. This agreement indicates that the dielectric constant can be understood in terms of a series capacitor model and that the Al_2O_3 ALE does not affect the electrical properties of the Al_2O_3 films.

The deposition and etchback approach can be used to increase the yield of fabricated devices based on ultrathin dielectric films. The improvement may result from the closure of pinholes by growing thicker films and then etching back to the ultrathin thickness. Some improvement may also be derived from the fluorination of the dielectric film that produces a volume expansion that closes pinholes resulting from compressive stress in the fluoride film. The number of pinholes in many other ultrathin films may be improved through a deposition and etchback process or through a surface treatment that produces a volume expansion.

ACKNOWLEDGMENTS

This research was supported by a contract from Sierra Nevada Corporation. The authors acknowledge useful discussions with Kevin Neitzel from Sierra Nevada Corporation. The authors thank Kristen Genter at NIST Boulder for the lithography masks. The authors also acknowledge the use of the JILA cleanroom at the University of Colorado Boulder for fabricating the MIM devices.

DATA AVAILABILITY

The data that support the findings of this study are available within the article.

REFERENCES

[1]S. M. George, Chem. Rev. **110**, 111 (2010).
[2]R. L. Puurunen, J. Appl. Phys. **97**, 121301 (2005).
[3]M. D. Groner, J. W. Elam, F. H. Fabreguette, and S. M. George, Thin Solid Films **413**, 186 (2002).
[4]E. P. Gusev, M. Copel, E. Cartier, I. J. R. Baumvol, C. Krug, and M. A. Gribelyuk, Appl. Phys. Lett. **76**, 176 (2000).
[5]J. Robertson and R. M. Wallace, Mater. Sci. Eng., R. **88**, 1 (2015).
[6]G. D. Wilk, R. M. Wallace, and J. M. Anthony, J. Appl. Phys. **89**, 5243 (2001).
[7]S. Jakschik, U. Schroeder, T. Hecht, M. Gutsche, H. Seidl, and J. W. Bartha, Thin Solid Films **425**, 216 (2003).
[8]J. A. Murdzek, A. Rajashekhar, R. S. Makala, and S. M. George, J. Vac. Sci. Technol. A **39**, 042602 (2021).
[9]A. Szeghalmi, M. Helgert, R. Brunner, F. Heyroth, U. Gosele, and M. Knez, Appl. Opt. **48**, 1727 (2009).
[10]P. F. Carcia, R. S. McLean, M. H. Reilly, M. D. Groner, and S. M. George, Appl. Phys. Lett. **89**, 031915 (2006).
[11]M. D. Groner, S. M. George, R. S. McLean, and P. F. Carcia, Appl. Phys. Lett. **88**, 051907 (2006).
[12]R. Cooper, H. P. Upadhyaya, T. K. Minton, M. R. Berman, X. H. Du, and S. M. George, Thin Solid Films **516**, 4036 (2008).
[13]B. Diaz, E. Harkonen, J. Swiatowska, V. Maurice, A. Seyeux, P. Marcus, and M. Ritala, Corros. Sci. **53**, 2168 (2011).
[14]N. D. Hoivik, J. W. Elam, R. J. Linderman, V. M. Bright, S. M. George, and Y. C. Lee, Sens. Actuators, A **103**, 100 (2003).
[15]C. F. Herrmann, F. H. Fabreguette, D. S. Finch, R. Geiss, and S. M. George, Appl. Phys. Lett. **87**, 123110 (2005).
[16]O. Hahtela, P. Sievila, N. Chekurov, and I. Tittonen, J. Micromech. Microeng. **17**, 737 (2007).
[17]J. Yota, H. Shen, and R. Ramanathan, J. Vac. Sci. Technol. A **31**, 01a134 (2013).
[18]D. Hoogeland, K. B. Jinesh, F. Roozeboom, W. F. A. Besling, M. de Sanden, and W. M. M. Kessels, J. Appl. Phys. **106**, 114107 (2009).
[19]R. T. Lu *et al.*, IEEE Trans. Appl. Supercond. **23**, 1100705 (2013).
[20]C. H. Chang, Y. K. Chiou, C. W. Hsu, and T. B. Wu, Electrochem. Solid-State Lett. **10**, G5 (2007).
[21]K. Kukli, M. Ritala, T. Pilvi, T. Aaltonen, J. Aarik, M. Lautala, and M. Leskela, Mater. Sci. Eng., B **118**, 112 (2005).
[22]A. Fischer, A. Routzahn, S. M. George, and T. Lill, J. Vac. Sci. Technol. A **39**, 030801 (2021).
[23]Y. Lee and S. M. George, ACS Nano **9**, 2061 (2015).
[24]S. M. George, Acc. Chem. Res. **53**, 1151 (2020).
[25]T. Faraz, F. Roozeboom, H. C. M. Knoops, and W. M. M. Kessels, ECS J. Solid State Sci. Technol. **4**, N5023 (2015).
[26]Y. Lee, J. W. DuMont, and S. M. George, Chem. Mater. **28**, 2994 (2016).
[27]Y. Lee, J. W. DuMont, and S. M. George, ECS J. Solid State Sci. Technol. **4**, N5013 (2015).
[28]Y. Lee and S. M. George, J. Vac. Sci. Technol. A **36**, 061504 (2018).
[29]J. W. DuMont, A. E. Marquardt, A. M. Cano, and S. M. George, ACS Appl. Mater. Interfaces **9**, 10296 (2017).
[30]Y. Lee and S. M. George, Chem. Mater. **29**, 8202 (2017).
[31]A. I. Abdulagatov and S. M. George, Chem. Mater. **30**, 8465 (2018).
[32]A. I. Abdulagatov and S. M. George, J. Vac. Sci. Technol. A **38**, 022607 (2020).
[33]N. R. Johnson and S. M. George, ACS Appl. Mater. Interfaces **9**, 34435 (2017).
[34]S. M. George and Y. Lee, ACS Nano **10**, 4889 (2016).
[35]D. R. Zywotko, J. Faguet, and S. M. George, J. Vac. Sci. Technol. A **36**, 061508 (2018).
[36]J. H. Klootwijk *et al.*, IEEE Electron Device Lett. **29**, 740 (2008).
[37]L. Strambini *et al.*, Nano Energy **68**, 104281 (2020).
[38]M. D. Groner, F. H. Fabreguette, J. W. Elam, and S. M. George, Chem. Mater. **16**, 639 (2004).
[39]J. C. Gertsch, A. M. Cano, V. M. Bright, and S. M. George, Chem. Mater. **31**, 3624 (2019).
[40]J. W. Elam, M. D. Groner, and S. M. George, Rev. Sci. Instrum. **73**, 2981 (2002).

[41]A. M. Cano, A. E. Marquardt, J. W. DuMont, and S. M. George, J. Phys. Chem. C **123**, 10346 (2019).
[42]Z. A. Sechrist, F. H. Fabreguette, O. Heintz, T. M. Phung, D. C. Johnson, and S. M. George, Chem. Mater. **17**, 3475 (2005).
[43]T. J. Myers, J. A. Throckmorton, R. A. Borrelli, M. O'Sullivan, T. Hatwar, and S. M. George, Appl. Surf. Sci. **569**, 150878 (2021).
[44]B. V. L'Vov, Thermochim. Acta **333**, 13 (1999).
[45]S. J. Schneider, *Compilation of the Melting Points of the Metal Oxides, Monograph 68* (National Bureau of Standards, Washington, D.C, 1963).
[46]N. Mahuli, A. S. Cavanagh, and S. M. George, J. Vac. Sci. Technol. A **39**, 022403 (2021).
[47]A. de Rooij, ESA J. **13**, 363 (1989).
[48]X. Y. Gao, H. L. Feng, J. M. Ma, Z. Y. Zhang, J. X. Lu, Y. S. Chen, S. E. Yang, and J. H. Gu, Phys. B **405**, 1922 (2010).
[49]X. H. Zhang, B. Domercq, X. D. Wang, S. Yoo, T. Kondo, Z. L. Wang, and B. Kippelen, Org. Electron. **8**, 718 (2007).
[50]X. Z. Li, M. Vehkamaki, M. Heikkila, M. Mattinen, M. Putkonen, M. Leskela, and M. Ritala, Coatings **11**, 355 (2021).
[51]A. S. Yersak and Y. C. Lee, J. Vac. Sci. Technol. A **34**, 01A149 (2016).